JOURNAL OF COMPUTATIONAL PHYSICS 86, 147–167 (1990)

# Implicit Solution of the Incompressible Navier–Stokes Equations on a Non-staggered Grid

M. L. MANSOUR AND A. HAMED

*Department of Aerospace Engineering and Engineering Mechanics,*
*University of Cincinnati,*
*Cincinnati, Ohio 45221–0070*

Received February 26, 1987; revised March 13, 1989

This paper presents an implicit procedure for the solution of the incompressible Navier–Stokes equations in primitive variables. The time dependent momentum equations are solved implicitly for the velocity field using the approximate factorization technique. The continuity equation is satisfied at each time step through the solution of a Poisson type equation for the static pressure. A consistent finite-difference scheme which satisfies the compatibility condition using a non-staggered grid is used in the finite difference approximation of the static pressure Poisson equation. The results of the numerical computations in a driven cavity, which are presented for the history of the residues, at several Reynolds numbers using different computational parameters, demonstrate the excellent convergence characteristics of the solution procedure. A stability analysis is conducted for the non-iterative phase and numerical results are presented for a given set of compational parameters. Numerical results obtained for the steady state static pressure in the driven cavity are presented for the first time at $Re = 1000$ using a non-staggered grid, and the steady state velocity, vorticity, and pressure contours at $Re = 100$, 400, and 1000, are compared with the computational results of other investigators. Additional results using a curvilinear grid are also presented for the flow in a cascade of circular airfoils at $Re = 1000$. 

## INTRODUCTION

The feasibility of obtaining an economical three-dimensional solution for the compressible Navier–Stokes equations has been demonstrated for laminar and turbulent flows in different geometries of practical interest [3–10]. Beam and Warming [11, 12] made a significant contribution through an implicit method for the coupled system of equations in conservation law form, which requires the solution of a block-tri-diagonal linear system. In their work they extended the ADI algorithm as done by Birley and McDonald [12] for the compressible Navier–Stokes equations to the coupled system of Euler equations. Shamrouth *et al.* [6] used the method of Briley and McDonald [12] to predict the cascade flow field using the averaged Navier–Stokes equations. Similar procedure was developed by MacCormack [13] in which he used a new non-centered method that requires only the solution of block-bi-diagonal linear system of equations. Lerat [14, 15] also proposed an implicit procedure that is space dissipative but similar to the Beam



0021-9991/90 $3.00

and Warming scheme. These two methods have been applied to compute the transonic flows over an airfoil by solving the Euler equations [16, 17].

The main obstacle in developing similar effective procedures for the solution of the incompressible Navier–Stokes equations is the absence of a time derivative in the continuity equation. On the other hand, the compressible N–S equations solution procedure cannot be used to compute an incompressible flow because of the singular behavior of the equations as the Mach number approach zero [18]. This leads to an ill-conditioned behavior and consequently very slow convergence. One of the important methods that has been used extensively, during the past decade, for solving the incompressible two-dimensional flow is the stream function vorticity formulation [19–21]. An inconvenience of this formulation is that the pressure is not directly obtained and consequently additional calculations are required for its determination.

There are two formulations that are valid for the solution of two- and three-dimensional incompressible flow equations, the artificial compressibility technique and the use of a Poisson equation for the pressure. Chorin [22] proposed the method of artificial compressibility to solve the incompressible flow equations. The approach modifies the continuity equation through the addition of a pressure–time derivative term which is divided by a parameter similar to the speed of sound. Steger and Kuttler [23] first used this method to compute the vortex wakes. Choi and Merkel [24] investigated the stability and the convergence characteristics of this method using the LBI scheme. They recommended that the factor of the time derivative term in the continuity equation be chosen near free stream velocity in order to speed up the convergence of the numerical solution. The same conclusion was arrived at by Rizzi and Erikson [25]. The use of such a low value for the pseudo speed of sound precludes the use of this formulation in transient problems, since the continuity equation is only satisfied at the steady state. If the continuity equation is to be satisfied at each time step, this pseudo speed of sound must be large [23], in which case the solution suffers slow convergence [25]. The incompressible flow momentum equations have also been solved in their primitive form along with a Poisson equation for the pressure [26]. The Poisson equation for the pressure is obtained by taking the divergence of the momentum equation. This was first presented by Harlow and Welch [27] in 1965 and Welch *et al.* [28] in conjunction with their Marker and Cell method. Earlier efforts at the numerical solution of the Poisson equation with Neumann boundary conditions using iterative methods on a non-staggered grid encountered difficulties since the compatibility condition that relates the source term of the pressure Poisson equation and the Neumann boundary conditions, through Green's theorem, is not satisfied [29]. Numerical fixes to this problem include the special treatment of the boundary conditions by Chorin [30] and the modification of the source of the Poisson equation by Briley [29]. The use of the staggered grid in the MAC method of Harlow and Welch [27] and Welch *et al.* [28] provided a remedy for the satisfaction of the compatibility condition.

Abdallah [1] proposed a consistent differencing scheme for the Poisson equation

and the Neumann boundary conditions, which numerically satisfies the compatibility condition on a non-staggered grid. Three main steps are involved in this scheme: first the viscous terms in the pressure boundary conditions are expressed in terms of the vorticity. Second, the pressure Poisson equation is used in conservative form. Third, the derivatives in the Poisson equation and its boundary conditions are discretized consistently. The convergence of this scheme was demonstrated by the solution of the primitive form of the N–S equations in the driven cavity [2]. Due to the explicit marching procedure that was used in the unsteady momentum equations, the highest Reynolds number that could be resolved was 400 on a $71 \times 71$ grid. In order to reach higher Reynolds numbers implicit time marching schemes are needed so that the time step is not restricted by the CFL condition. Also, the solution of the momentum equations in coupled form provides better convergence and deals effectively with the very stiff and ill-conditioned system of equations, at high Reynolds numbers.

In the present work a consistent finite differencing scheme is developed for the pressure Poisson equation in general curvilinear coordinates and is combined with an implicit scheme for solving the coupled momentum equations on a non-staggered grid. The procedure is presented for two-dimensional flows but its extension to three-dimensional flow is straightforward. The equations for the numerical solution are first order in time [11], however second-order schemes can be used as demonstrated in Ref. [7]. A standard von Neumann linearized stability analysis is performed for the noniterative phase of the two-dimensional algorithm, and the numerical results are presented. The convergence characteristics for the numerical procedure are presented for the driven cavity problem, which has served as a standard test case for almost every new innovation associated with the incompressible N–S equations. Numerical solutions are obtained for flow Reynolds numbers up to 1000 in a driven cavity and in a cascade of symmetric airfoils. The results for the computed pressure, vorticity, and the velocity profiles in the driven cavity compare very favorably with the computational results of other methods using much finer grids [32, 36]. Results which are presented for the residues in the numerical scheme, at different CFL conditions and different Reynolds numbers, show excellent convergence characteristics. Furthermore, it is also demonstrated that the combination of the pressure Poisson equation with the implicit coupled schemes is superior to the explicit and uncoupled schemes.

## Governing Equations

The governing equations for the time dependent incompressible laminar flow are written in strong conservation law form, in general curvilinear coordinates $(\xi, \eta)$, using the general transformation by Viviand [33] and Vinokur [34],

$$\partial_t q/J + \partial_\xi E + \partial_\eta F = R_e^{-1} \nabla^2 q, \tag{1}$$

where

$$q = (u, v)^{\mathrm{T}}$$

$$J = 1 \Big/ \frac{\partial(x, y)}{\partial(\xi, \eta)}$$

$$E = J^{-1}(uU + \xi_x p, vU + \xi_y p)^{\mathrm{T}}$$

$$F = J^{-1}(uV + \eta_x p, vV + \eta_y p)^{\mathrm{T}}$$

and

$$\nabla^2 = \partial_\xi(J^{-1}\nabla\xi \cdot \nabla\xi)\,\partial_\xi + \partial_\xi(J^{-1}\nabla\xi \cdot \nabla\eta)\,\partial_\eta + \partial_\eta(J^{-1}\nabla\xi \cdot \nabla\eta)\,\partial_\xi + \partial_\eta(J^{-1}\nabla\eta \cdot \nabla\eta)\,\partial_\eta.$$

In the above equations, $u$ and $v$ are the Cartesian velocity components while $U$ and $V$ are the contravariant velocity components defined as

$$U = \xi_x u + \xi_y v$$

and

$$V = \eta_x u + \eta_y v. \tag{2}$$

The Poisson equation for the pressure is obtained by taking the divergence of the unsteady momentum equations and using the continuity equation to eliminate the viscous terms [26]. Upon applying the general coordinate transformation [33, 34], the Poisson equation for the static pressure is expressed in general curvilinear coordinates as

$$\partial_\xi(\alpha p_\xi + \gamma p_\eta + \sigma_1) + \partial_\eta(\beta p_\eta + \gamma p_\xi + \sigma_2) + \partial_t D = 0, \tag{3}$$

where

$$\alpha = J^{-1}\nabla\xi \cdot \nabla\xi,$$

$$\beta = J^{-1}\nabla\eta \cdot \nabla\eta,$$

$$\gamma = J^{-1}\nabla\xi \cdot \nabla\eta,$$

$$D = \left(\frac{U}{J}\right)_\xi + \left(\frac{V}{J}\right)_\eta,$$

$$\sigma_1 = J^{-1}(\xi_x U u_\xi + \xi_x V u_\eta + \xi_y U v_\xi + \xi_y V v_\eta),$$

and

$$\sigma_2 = J^{-1}(\eta_x U u_\xi + \eta_x V u_\eta + \eta_y U v_\xi + \eta_y V v_\eta).$$

As suggested by Harlow and Welch [27], the dilation term, $D$, is retained in Eq. (3) in order to avoid the numerical instability.

Equation (3) is a second-order elliptic partial differential equation which is solved for the static pressure. The conservative form of this equation is necessary for the consistent finite differencing scheme which will be discussed later.

*Boundary Conditions*

The Neumann boundary conditions for the pressure are obtained from the momentum equations. A solution for the Poisson equation with Neumann boundry conditions, exists only if a compatibility condition is satisfied. This compatibility condition results from Green's theorem which relates the source term of the Poisson equation and its Neumann boundary conditions as

$$-\iint_A (\partial_\xi \sigma_1 + \partial_\eta \sigma_2)\, dA = \int_c \frac{\partial p}{\partial n}\, ds, \tag{4}$$

where $(\partial_\xi \sigma_1 + \partial_\eta \sigma_2 + J^{-1}\partial_t D)$ is the source term of the Poisson equation, $c$ is the contour enclosing the area of solution domain $A$, and $n$ is the outward normal to the boundary $c$. This condition is not automatically satisfied on a non-staggered grid [26]. A consistent finite difference scheme for the pressure equation and its boundary conditions that satisfies the compatibility condition on a non-staggered grid, which was proposed by Abdallah [1, 2] in cartesian coordinates, is extended here to the general curvilinear coordinate.

The boundary conditions for the static pressure Poisson equation are obtained from the momentum equations after replacing the Laplacian of the velocities (diffusion term) by the curl of the vorticity. At the constant $\eta$-boundaries the pressure boundary conditions are obtained from the relation

$$(\nabla\xi \cdot \nabla\xi)\, p_\xi + (\nabla\xi \cdot \nabla\eta)\, p_\eta = -\partial_t U - \xi_x(Uu_\xi + Vu_\eta) - \xi_y(Uv_\xi + Vv_\eta) - JR_e^{-1}\Omega_\eta \tag{5}$$

while the boundary condition at constant $\xi$-boundary is obtained from the equation

$$(\nabla\eta \cdot \nabla\eta)\, p_\eta + (\nabla\xi \cdot \nabla\eta)\, p_\xi = -\partial_t V - \eta_\xi(Uu_\xi + Vu_\eta) - \eta_\eta(Uv_\xi + Vv_\eta) + JR_e^{-1}\Omega_\xi. \tag{6}$$

In the above equations the vorticity $\Omega$ is expressed in terms of the velocity in conservative form as

$$\Omega = J\{(J^{-1}\xi_x v - J^{-1}\xi_y u)_\xi - (J^{-1}\eta_y u - J^{-1}\eta_x v)_\eta\}. \tag{7}$$

## Numerical Solution

The present procedure for solving the incompressible Navier–Stokes equations consists of two steps at each time level. In the first step the momentum equations are solved implicitly in coupled form, using the method of approximate factorization [11], to get the velocity field at the new time level. In the second step the Poisson equation for the static pressure is solved iteratively using the method of point SOR.

*The Velocity Field*

The Euler implicit differencing method is used for the time marching of the momentum equations. The semi-discretized form of the equations, after the approximate factorization of Beam and Warming [11] is

$$[I+J\Delta t(\partial_\xi A^n - IR_e^{-1}\partial_\xi \nabla\xi\cdot\nabla\xi\,\partial_\xi)][I+J\Delta t(\partial_\eta B^n - IR_e^{-1}\partial_\eta\nabla\eta\cdot\nabla\eta\,\partial_\eta)]\,\Delta q^n$$
$$= J\Delta t\{-(\partial_\xi E_1^n + \partial_\eta F_1^n) + R_e^{-1}(D_{\xi\xi}+D_{\xi\eta}+D_{\eta\eta}+D_{\eta\xi})\,q^n$$
$$+ R_e^{-1}(D_{\xi\eta}+D_{\eta\xi})\,\Delta q^{n-1}\}, \tag{8}$$

where

$$D_{\xi\xi} = \partial_\xi \nabla\xi\cdot\nabla\xi\,\partial_\xi,$$
$$D_{\xi\eta} = \partial_\xi \nabla\xi\cdot\nabla\eta\,\partial_\eta,$$
$$D_{\eta\eta} = \partial_\eta \nabla\eta\cdot\nabla\eta\,\partial_\eta,$$
$$D_{\eta\xi} = \partial_\eta \nabla\xi\cdot\nabla\eta\,\partial_\xi,$$
$$\Delta q^n = q^{n+1} - q^n,$$

and

$$\Delta q^{n-1} = q^n - q^{n-1}.$$

$\Delta q^{n-1}$ appears on the right-hand side of Eq. (8) as a result of time lagging the cross derivatives of the vector, $q$, one time step.

In order to be compatible with the implicit algorithm, the linearization of the flux vectors $E$ and $F$ results in defining the flux vectors jacobian matrices, $A^n$ and $B^n$ in the form

$$A^n = \partial E/\partial q = J^{-1}\begin{vmatrix} 2u\xi_x+\xi_y v & \xi_y u \\ \xi_x v & 2\xi_y v+\xi_x u \end{vmatrix} \tag{9}$$

and

$$B^n = \partial F/\partial q = J^{-1}\begin{vmatrix} 2u\eta_x+\eta_y y & \eta_y u \\ \eta_x v & 2\eta_y v+\eta_x u \end{vmatrix}. \tag{10}$$

Equation (8) represents the semi-discretized form of the momentum equations which is solved for the velocity field, $q$. This solution is performed in two steps; each involves a solution of a one-dimensional block tri-diagonal matrix inversion. In the discretization of Eq. (8), the operators in the convection terms $\partial_\xi$ and $\partial_\eta$ are approximated using second-order central differencing expressions. The use of the second-order space central differencing for the convection terms is responsible for introducing high frequency oscillations in the numerical solution. These high frequency oscillations can be suppressed by adding an explicit fourth-order dissipation term to the right-hand side of the momentum equation, Eq. (8). This term can be

written in the form: $-(\omega/16)(\Delta\xi^4\partial_{\xi\xi\xi\xi}+\Delta\eta^4\partial_{\eta\eta\eta\eta})\,q^n$. The presence of this fourth-order term has only a minor impact on the second-order physical viscosity term, in contrast to up-winding schemes which introduce second-order artificial viscosity. The finite differencing approximation of the viscous terms is also performed using second-order expressions. Referring to Fig. (1), any one term of the form $\partial_\xi a\,\partial_\xi b$ is differenced as

$$\partial_\xi a\,\partial_\xi b=[a_e(b_{i+1,j}-b_{i,j})-a_w(b_{i,j}-b_{i-1,j})]/(\Delta\xi)^2, \tag{11}$$

where $e$ and $w$ refer to the east and the west stations, respectively, as shown in Fig. 1.

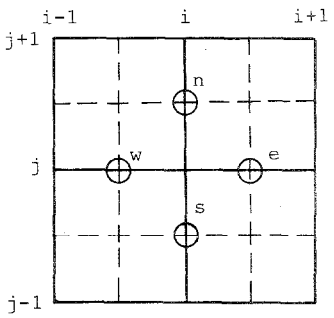


(a) Discretization Cell

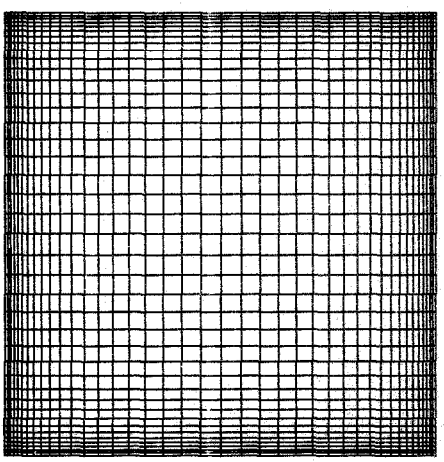

b) Clustered Grid

FIG. 1. Discretization cell and the grid.

*The Pressure Field*

The Poisson equation for the static pressure, Eq. (3), is solved iteratively at every time level. This equation and its boundary conditions are consistently discretized [1] in order to satisfy the compatibility condition. Referring to Fig. 1 the discretized form of Eq. (3) is written as

$$\{[\alpha p_\xi + \gamma p_\eta]_e - [\alpha p_\xi + \gamma p_\eta]_w\}^n - \{[\gamma p_\xi + \beta p_\eta]_n - [\gamma p_\xi + \beta p_\eta]_s\}^n + [\sigma_{1e} - \sigma_{1w} + \sigma_{2n} - \sigma_{2s}] = D^n/\Delta t. \tag{12}$$

The finite difference approximation of the terms on the left-hand side of Eq. (12) are then discretized at $e$, $n$, $w$, and $s$ as shown in Fig. 1 using second-order central difference approximations:

$$(\alpha p_\xi)_e = \alpha_e (P_{i+1,j} - P_{i,j}) \tag{13}$$

$$(\gamma p_\eta)_e = \tfrac{1}{4}\gamma_e (p_{i+1,j+1} + P_{i,j+1} - P_{i+1,j-1} - P_{i,j-1}) \tag{14}$$

$$\sigma_{1e} = J_e^{-1}(\xi_{xe} U_e u_{\xi e} + \xi_{xe} V_e u_{\eta e} + \xi_{ye} U_e v_e + \xi_{ye} V_e v_{\eta e}). \tag{15}$$

Similar expressions at the west, north, and south stations can be obtained using the same procedure leading to the discrete form for the pressure equation,

$$\begin{aligned} &-(\alpha_e + \alpha_w + \beta_n + \beta_s)\, p_{i,j} + (\alpha_w + (\gamma_s - \gamma_n)/4)\, p_{i-1,j} + (\alpha_e + (\gamma_n - \gamma_s)/4)\, p_{i+1,j} \\ &+ (\beta_s + (\gamma_w - \gamma_e)/4)\, p_{i,j-1} + (\beta_n + (\gamma_e - \gamma_w)/4)\, p_i + ((\gamma_w + \gamma_s)/4)\, p_{i-1,j-1} \\ &+ ((\gamma_e + \gamma_n)/4)\, p_{i+1,j+1} - ((\gamma_w + \gamma_n)/4)\, p_{i-1,j+1} - ((\gamma_e + \gamma_s)/4)\, p_{i+1,j-1} \\ &+ \sigma_{i,j} = D^n/\Delta t, \end{aligned} \tag{16a}$$

where

$$\sigma_{i,j} = \sigma_{1e} - \sigma_{1w} + \sigma_{2n} - \sigma_{2s}. \tag{16b}$$

*Boundary Conditions*

The Neumann boundary conditions represented by Eqs. (5) and (6), are discretized at half-grid spacing from the boundaries. The expression for the boundary condition along the left boundary, at $\xi = 0$ $(i = 1)$ is

$$\begin{aligned} &(J\alpha)_{e,j}\,(p_{2,j} - p_{1,j}) - \frac{1}{4}(J\gamma)_{e,j}\,(p_{2,j+1} + p_{1,j+1} - p_{2,j-1} - p_{1,j-1}) \\ &\quad = \frac{1}{2}(\sigma_{1_{1,j}} + \sigma_1)_{1,j} + R_e^{-1}\frac{1}{4}(\Omega_{2,j+1} + \Omega_{1,j+1} - \Omega_{2,j-1} - \Omega_{1,j-1}) \\ &\qquad - \frac{1}{2\,\Delta t}[(J^{-1}U)_{1,j} + (J^{-1}U)_{2,j} - (J^{-1}U)_{1,j} - (J^{-1}U)_{2,j}]. \end{aligned} \tag{17}$$

The boundary conditions along the other three boundaries can be obtained using similar equations.

The outlined finite differencing procedure for the pressure equation and boundary condition satisfies the compatibility condition in discrete form. This can be easily proven by adding Eq. (16b) and the discrete form of the equations for the boundary conditions, represented by Eq. (17).

*Transformation Parameters*

The consistent finite difference approximations for the pressure Poisson equation and the Neumann boundary conditions, Eqs. (16) and (17), require calculation of the metric coefficients $\xi_x$, $\xi_y$, $\eta_x$, and $\eta_y$ as well as the Jacobian of the transformation, $J$, at the locations $e$, $w$, $n$, and $s$. Also, the finite difference approximation in the diffusion terms in the momentum equation, as expressed in Eq. (11) requires the calculation of the same coefficients and the velocity components at the same locations, Fig. 1. A simple averaging procedure is used for the velocity components at thes locations, but the metric coefficients and the Jacobian are determined from a dual grid to exactly satisfy the metric identities [36]. Figure 1b shows the clustered grid that was used.

## Stability Analysis for the Non-iterative Phase

The von Neumann stability analysis is conducted for the momentum equations represented by Eq. (8) and does not take into account the coupling between the momentum equations and the pressure Poisson equation. For simplicity, the two-dimensional equations are considered in cartesian coordinates. Assuming that the momentum equation flux vectors are homogeneous functions of the vector ($q$) and the flux vectors Jacobian matrices $A^n$ and $B^n$ are constants, the approximate factorized momentum equations, can be written as

$$[I+\Delta t(A^n\partial_x - I\mathrm{Re}^{-1}\partial_{xx})][I+\Delta t(B^n\partial_y - I\mathrm{Re}^{-1}\partial_{yy})]\,\Delta q^n$$
$$= -\Delta t(A^n\partial_x + B^n\partial_y)\,q^n + \mathrm{Re}^{-1}\,\Delta t\,\nabla^2 q^n - \frac{\omega}{16}(\Delta x^4\partial_{xxxx} + \Delta y^4\partial_{yyyy})\,q^n. \quad (18)$$

The last term on the right-hand side of the above equation represents the fourth-order dissipation term which is added in the numerical solutions. Expanding the left-hand side of the above equation and expressing $\Delta q^n$ as the difference between $q^{n+1}$ and $q^n$ one obtains

$$\{I+\Delta t\,A^n\partial_x+\Delta t\,B^n\partial_y-\Delta t\,I\,\mathrm{Re}^{-1}\partial_{xx}-\Delta t\,I\,\mathrm{Re}^{-1}\partial_{yy}$$
$$+\Delta t^2(A^nB^n\partial_{xy}-\mathrm{Re}^{-1}A^n\partial_{xyy}-\mathrm{Re}^{-1}B^n\partial_{xxy}+I\,\mathrm{Re}^{-2}\partial_{xxyy})\}\,sq^{n+1}$$
$$=\{I+\Delta t^2(A^nB^n\partial_{xy}-\mathrm{Re}^{-1}A^n\partial_{xyy}-\mathrm{Re}^{-1}B^n\partial_{xxy}+I\,\mathrm{Re}^{-2}\partial_{xxyy})\}\,q^n$$
$$=-\frac{\omega}{16}(\Delta x^4\partial_{xxxx}+\Delta y^4\,\partial_{yyyy})\,q^n. \quad (19)$$

In conducting the stability analysis for Eq. (19), the solution at the new time step is considered as a multiplication of the solution at the old time step and an amplification matrix, $G$,

$$q^{n+1} = Gq^n. \tag{20}$$

In order for the system to be stable, the eigenvalues of the $G$ matrix should be less than unity. As can be seen from Eq. (19) the approximate factorization adds new term of order $\Delta t^2$. Using a double Fourier decomposition for the solution $q^n$, the central difference version of Eq. (19) gives

$$LG = R, \tag{21}$$

where

$$\begin{aligned} L = I &+ i\frac{\Delta t}{\Delta x} A^n \sin\psi + i\frac{\Delta t}{\Delta y} B^n \sin\phi - 2\frac{\Delta t}{\Delta x^2} I\,\mathrm{Re}^{-1}(\cos\psi - 1) \\ &- 2\frac{\Delta t}{\Delta y^2} I\,\mathrm{Re}^{-1}(\cos\phi - 1) + \Delta t^2\left[ -\frac{A^n B^n}{\Delta x\,\Delta y}\sin\psi\sin\phi \right. \\ &- 2i\,\mathrm{Re}^{-1}\frac{A^n}{\Delta x\,\Delta y^2}\sin\psi(\cos\phi - 1) - 2i\,\mathrm{Re}^{-1}\frac{B^n}{\Delta y\,\Delta x^2}\sin\phi(\cos\psi - 1) \\ &\left. + 4I\,\mathrm{Re}^{-2}\frac{1}{\Delta x^2\,\Delta y^2}(1-\cos\psi)(1-\cos\phi)\right] \end{aligned} \tag{22}$$

and

$$\begin{aligned} R = I &+ \Delta t^2\left[ -\frac{A^n B^n}{\Delta x\,\Delta y}\sin\psi\sin\phi - 2i\,\mathrm{Re}^{-1}\frac{A^n}{\Delta x\,\Delta y^2}\sin\psi(\cos\phi - 1) \right. \\ &- 2i\,\mathrm{Re}^{-1}\frac{B^n}{\Delta y\,\Delta x^2}\sin\phi(\cos\psi - 1) \\ &\left. + 4I\,\mathrm{Re}^{-2}\frac{1}{\Delta x^2\,\Delta y^2}(1-\cos\psi)(1-\cos\phi)\right] \\ &- I\frac{\omega}{8}[6 - 4(\cos\psi + \cos\phi) + \cos 2\psi + \cos 2\phi)]. \end{aligned} \tag{23}$$

Considering a large wave number characteristic for the matrix $G$ by taking the values of the Fourier components $\psi$ and $\phi$ at the upper limit, $\pi$, the matrices $L$ and $R$ simplify and two equal eigenvalues are obtained,

$$e_{1,2} = \frac{1 - 2\omega + a/\mathrm{Re}^2}{[1 + 4b/\mathrm{Re} + a/\mathrm{Re}^2]}, \tag{24}$$

where $a = 16\Delta t^2/\Delta^2 x/\Delta^2 y$ and $b = \Delta t(1/\Delta^2 x + 1/\Delta^2 y)$.

It is easy to see from Eq. (24) that $|e_{1,2}| \leq 1$ for $0 \leq \omega \leq 1$ at any Reynolds

## Results and Discussion

The presented results consist of two parts, the first is concerned with the demonstration of the convergence and stability characteristics of the numerical scheme, while in the second the computed steady state pressure velocity and vorticity are compared with results of other methods.

Two parameters were investigated to study their influence on the convergence characteristics of the numerical solution in a square driven cavity. These parameters are the maximum number of iterations allowed in the solution of the pressure equation, IP, and the CFL number ($U\,\Delta t/\Delta x$). Both parameters influence the number of time steps required to achieve a certain convergence criterion. The following convergence criterion is adopted in this study:

$$\varepsilon = \frac{1}{MN} \sum_{j=1}^{M} \sum_{i=1}^{N} |a^{n+1} - a^n|. \tag{25}$$

The above equation represents the residue, $\varepsilon$, in the computed variables, $p$, $u$, and $v$, which was taken less than or equal to $10^{-7}$. The results of the convergence characteristics are presented in Fig. 2 through 4 and summarized in Table I.

Figures 2 and 3 show the convergence characteristics for $\mathrm{Re} = 100$, using a uniform $41 \times 41$ grid and no artificial dissipation ($\omega = 0$). Figure 2 demonstrates the change in the log norm of the residues for $p$, $u$, and $v$ with time, when the maximum number of iterations in the pressure solution, IP, was fixed at 5 and 10. In both cases the CFL was taken to be 2. One can observe from Fig. 2 that the reduction of the maximum number of iterations for the pressure to 5 increases the oscillations in the residues of the velocities. These oscillations are not drastic, however, and the

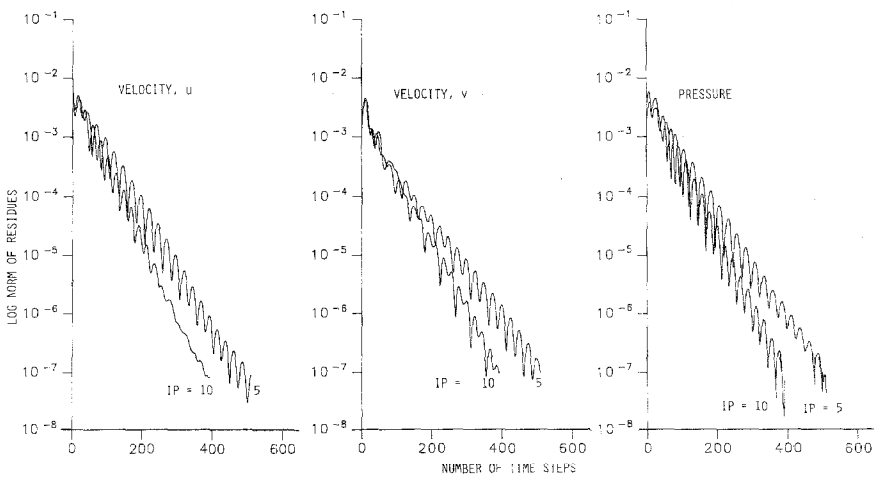


Fig. 2. Effect of IP on the convergence history for $\mathrm{Re} = 100$, $\omega = 0$, and $\mathrm{CFL} = 2$.

TABLE I

Solution Convergence Summary

| Re | 100 | 100 | 100 | 100 | 100 | 400 | 1000 |
|---|---|---|---|---|---|---|---|
| CFL | 2 | 2 | 5 | 10 | 20 | 1–17 | 1–17 |
| $\omega$ | 0 | 0 | 0 | 0 | 0 | 0.8 | 1.0 |
| IP | 5 | 10 | 10 | 10 | 10 | 10 | 10 |
| Time steps to convergence | 512 | 384 | 286 | 299 | 438 | 840 | 1400 |

solution still converges with a linear variation in $\log(\varepsilon)$ with time steps. The convergence rate with the time steps is higher when a larger number of iterations is allowed in the solution of the pressure equation. The effect of the CFL number on the solution convergence characteristics is presented in Fig. 3, which shows the change in the log norm of the residues with the number of time steps for CFL = 2, 5, and 20. One can observe a higher convergence rate at CFL = 5. This and other results at CFL = 10, as summarized in Table I, suggest an optimum value of CFL between 5 and 10. Figures 2 and 3 show the linear variation of $\log(\varepsilon)$ with the number of time steps and clearly demonstrate the excellent convergence characteristics of the present method under varying conditions. The rest of the results at $R_e = 400$ and 1000 were obtained using a clustered grid as shown in Fig. 1. The non-uniform grid used in the calculation is exponentially graded with the smallest grid spacing next to the wall equal to 0.003, of the cavity's characteristic length. A fixed time step of 0.05 was used with a maximum of 10 iterations allowed for the pressure equation at each time step. For $R_e = 400$ and 1000 the dissipation factor, $\omega$, was taken to be 0.8 and 1.0, respectively. A comparison of the convergence

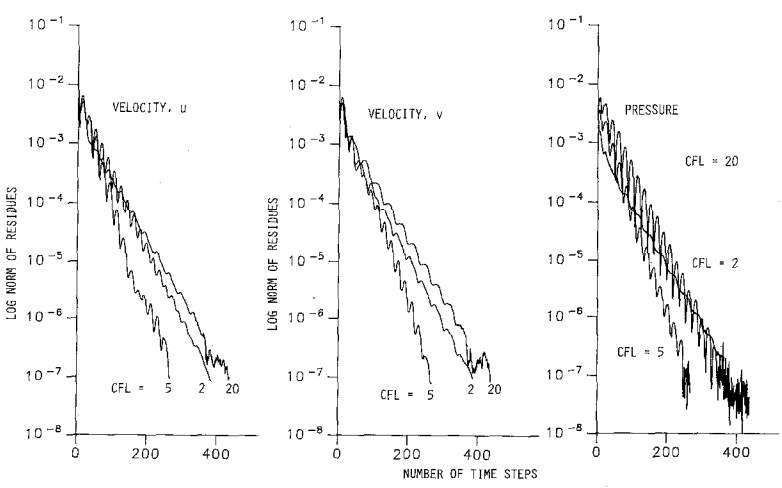


FIG. 3. Effect of CFL on the convergence history for Re = 100, $\omega = 0$, and IP = 10.

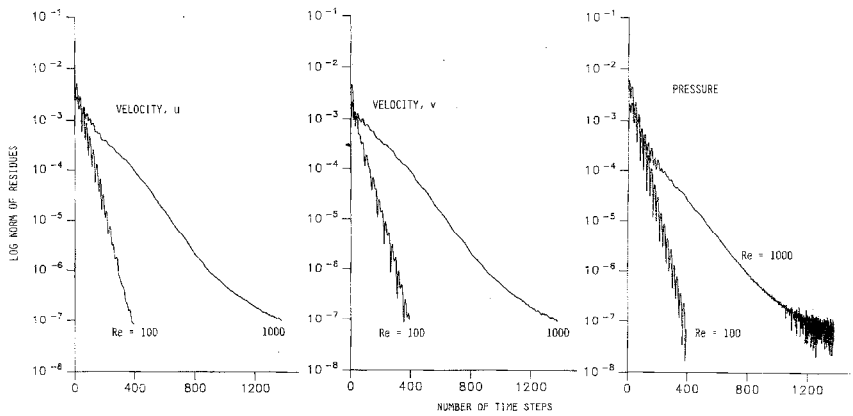


FIG. 4. Effect of Re on the convergence history.

histories for Reynolds numbers, 100 and 1000, is presented in Fig. 4. One can observe from this figure that when the coefficient of the fourth-order dissipation term is not zero the oscillations in the velocity residues are greatly reduced with a consequent improvement in the pressure residue as well.

A stability analysis has been conducted based on Eqs. (21) to (23), and the results of a numerical study of the amplification matrix are presented in Figs. 5 through 7. These figures show the contours of the modulus of the two eigenvalues of the amplification matrix over wave numbers, $\phi$ and $\psi$, ranging between zero and $\pi$. Figure 5 gives the results of the stability analysis for $\mathrm{Re} = 100$, with no artificial dissipation ($\omega = 0$), at the location in the cavity corresponding to the grid point (3, 3) near the left-hand corner of the upper moving wall. This figure demonstrates that the eigenvalues of the amplification matrix are equal to one at $\phi = 0$ and $\psi = 0$, but are less than one for all other $\phi$ and $\psi$ values. Figures 6 and 7 present the effect of the fourth-order dissipation coefficient $\omega$ on the two eigenvalues for $\mathrm{Re} = 400$ at the (31, 21) location. One can see from these figures that $\omega$ generally reduces the

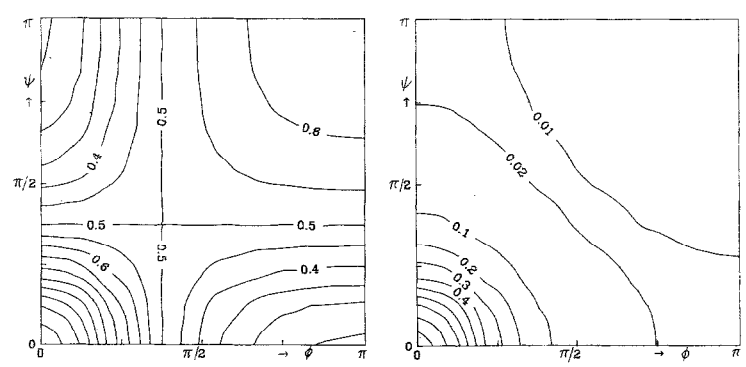


FIG. 5. Modulus of the eigenvalue of the amplification matrix for $\mathrm{Re} = 100$ and $\mathrm{CFL} = 2$.

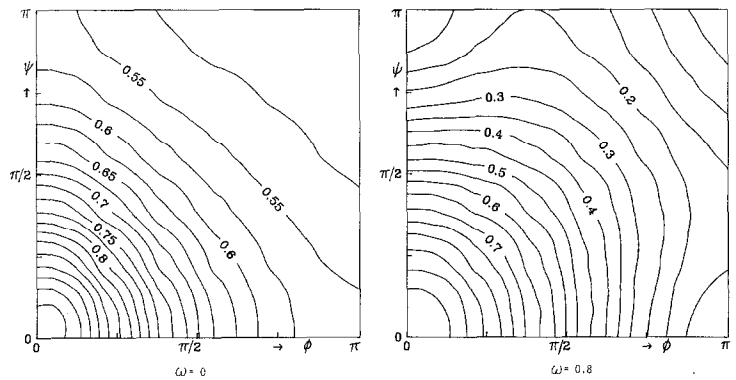


FIG. 6. Effect of $\omega$ on the modulus of the first eigenvalue of the amplification matrix at $\mathrm{Re} = 400$.

modulus of both eigenvalues over the range of the wave numbers, except at $\phi = \psi = 0$, where the eigenvalues are always equal to one. The results of the stability analysis are not presented at higher Reynolds number since the numerical study of the amplification matrix was conducted using a uniform nonclustered grid.

The results for the computed vorticity, velocities, and pressure in the driven cavity are presented in Figs. 8 through 15 for Reynolds numbers 100, 400, and 1000. The computed results are compared with the available results of other investigators, in order to validate the accuracy of the numerical procedure. The vorticity contours and the velocity profiles are presented together with the results of other investigators [19, 32], in Figs. 8 through 12. Both studies obtained their results using the stream function vorticity formulation, Burggraf [19] used $41 \times 41$ grid and Schreiber [32] used $180 \times 180$ grid and a fourth-order accurate technique. One can observe the agreement between the computed vorticity contours and Burggraf's [19] results at $\mathrm{Re} = 100$ and Schreiber's [32] at $\mathrm{Re} = 400$ and 1000. The velocity profiles for $u$ and $v$ $\mathrm{Re} = 1000$ are compared with the results by

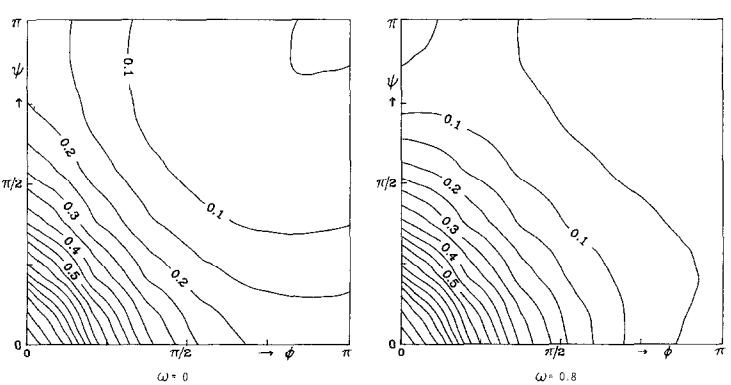


FIG. 7. Effect of $\omega$ on the modulus of the second eigenvalue of the amplification matrix at $\mathrm{Re} = 400$.

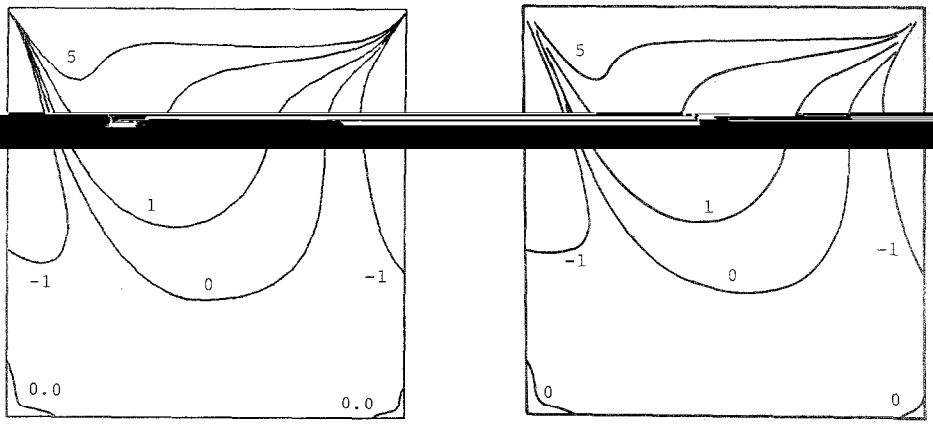


Present Results Results of Reference (19)

FIG. 8. Vorticity contours at Re = 100.

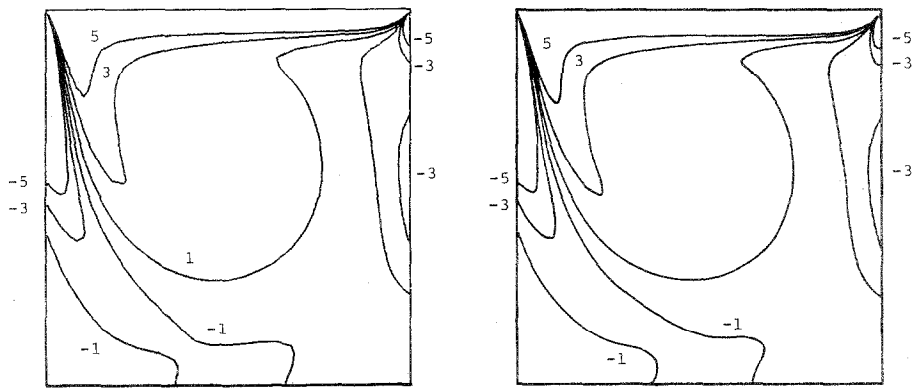


Results of Reference (32)

FIG. 9. Vorticity contours at Re = 400,

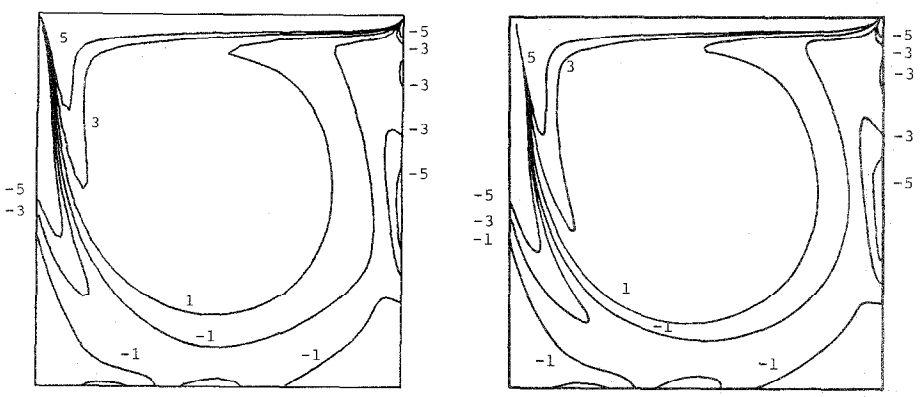


Present Results Results of Reference (32)

FIG. 10. Vorticity contours at Re = 1000.

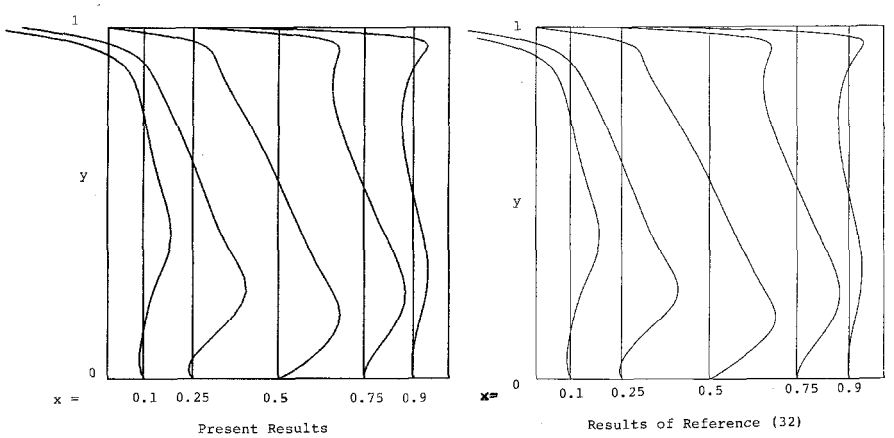


FIG. 11. Velocity profiles for the velocity component, $u$, at $Re = 1000$.

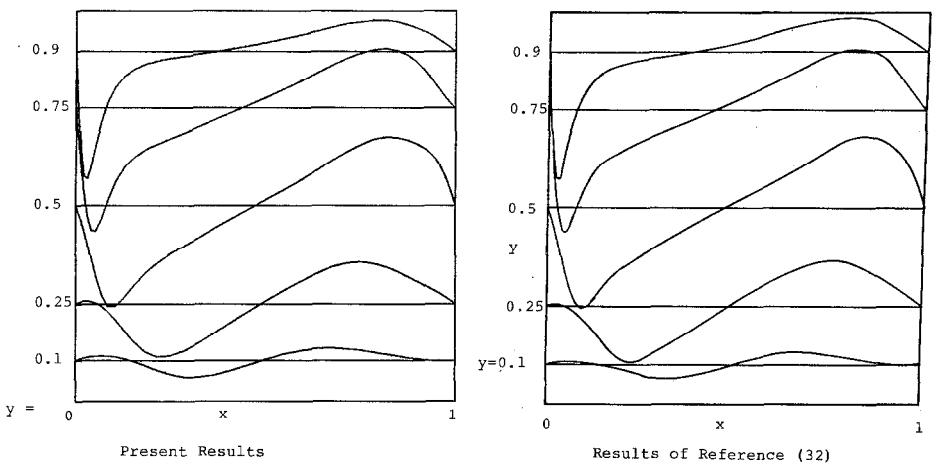


FIG. 12. Velocity profiles for the velocity component, $v$, at $Re = 1000$.

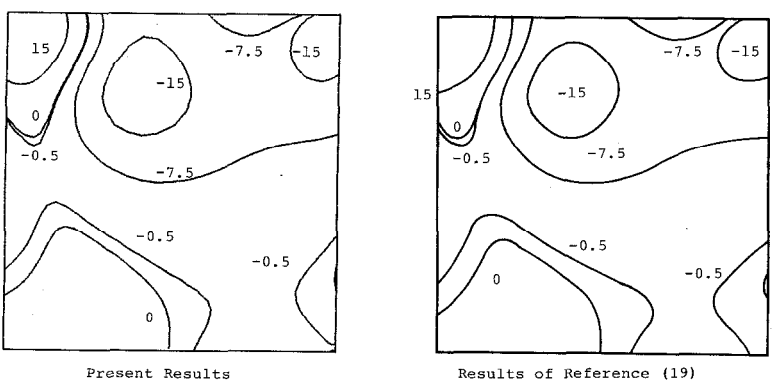


FIG. 13. Pressure coefficient contours at $Re = 100$.

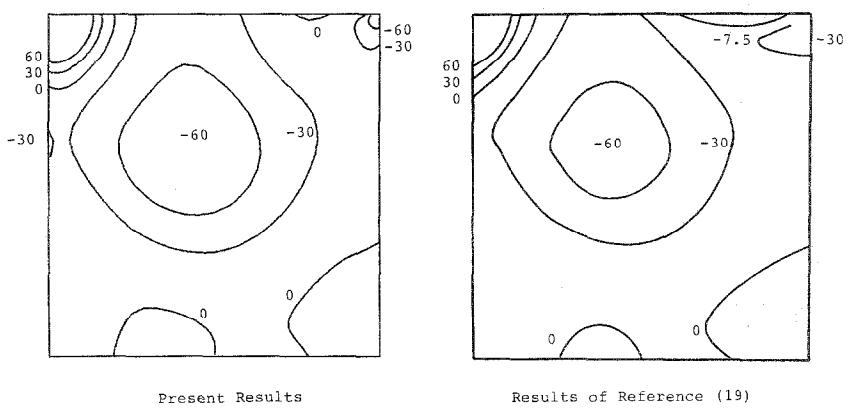


FIG. 14. Pressure Coefficient contours at Re = 400.

Schreiber [32] in Figs. 11 and 12. The comparison shows excellent agreement even though a relatively coarse grid was used in the present computations.

Figures 13 through 15 present the computed static pressure coefficient and the results of Res. [17, 36], at Re = 100, 400, and 1000. The numerical solution for the pressure in Ref. [36] was obtained on a $69 \times 69$ staggered grid. The static pressure coefficient is defined as

$$C_p = 2(p - p_0)/U^2, \tag{26}$$

where $p_0$ is the reference pressure at the center of the cavity's lower boundary and $U$ is the cavity's upper surface velocity. One can see that the results of the present method are in excellent agreement with the results obtained by Burggraf [17] at 100 and 400 Reynolds numbers. The computed static pressure coefficient at Re = 1000 is shown in Fig. 15, with the results of Ref. [36].

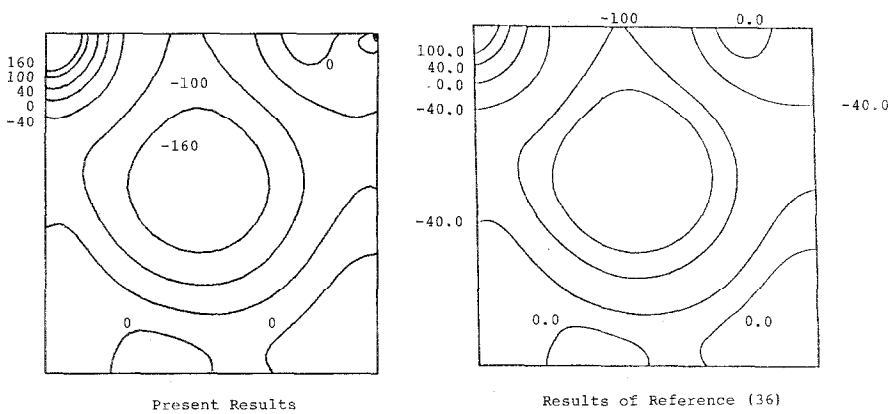


FIG. 15. Pressure coefficient contours at Re = 1000.

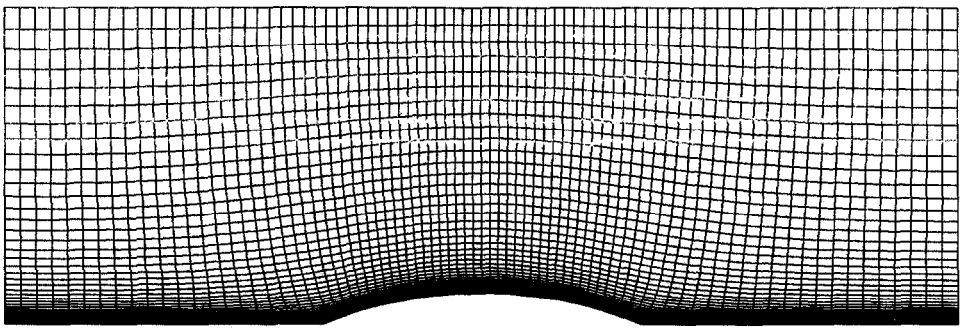

FIG. 16. The clustered grid for the cascade flow.

Numerical solutions for the steady state flow in the circular arc cascade were obtained at Reynolds number up to $Re = 1000$. The configuration corresponds to a thickness to chord ratio of 0.2 and pitch to chord ratio of 2.0. Figure 16 shows the $81 \times 41$ clustered grid used in the lower half of the symmetric blade to blade flow passage. The grid was generated using the Poisson equation approach of Ref. [37]. The smallest grid spacing next to the wall was equal to 0.005 of the cascade pitch. A maximum of 10 iterations were allowed in the solution of the elliptic pressure equation at each time step, but only one or two iterations were required to bring

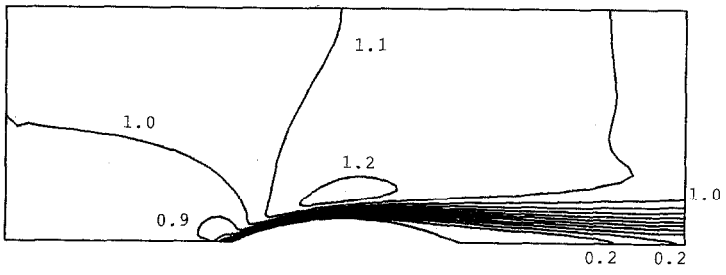


Present Results

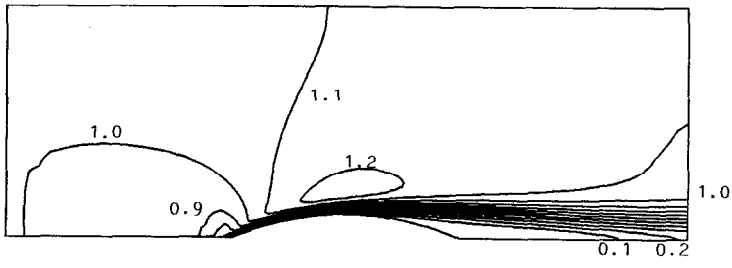


Results of Reference (32)

FIG. 17. Velocity contours for the cascade flow at $Re = 1000$.

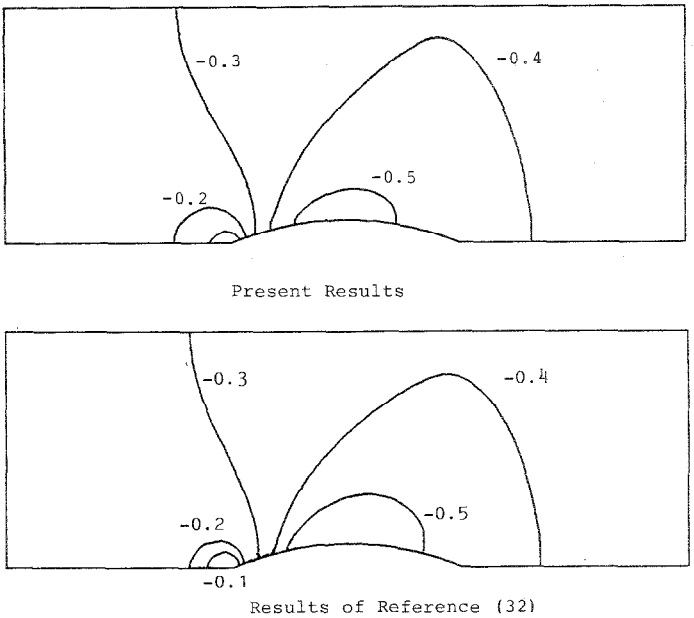


FIG. 18. Pressure coefficient contours for cascade flow at Re = 1000.

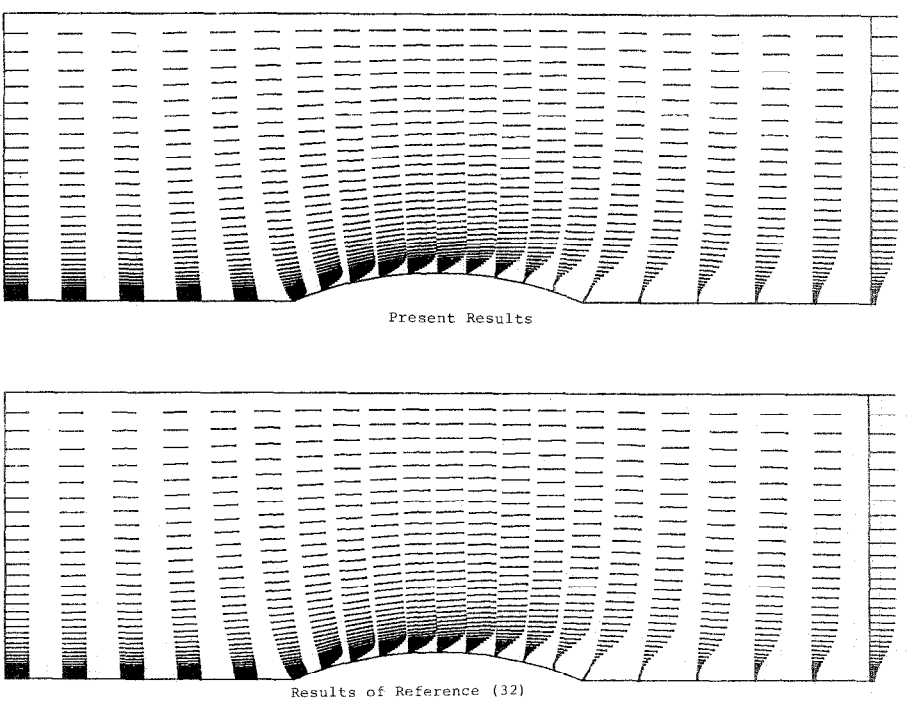


FIG. 19. Velocity profiles for the cascade flow at Re = 1000.

the residue back within the convergence criterion near the steady state. The computed results for the cascade are compared with the results using the artificial compressibility method in Figs. 17 through 19, A factored ADI scheme, similar to that given by Eq. (8), was developed for the implicit solution of the momentum and continuity equation in the artificial compressibility formulation. Figures 17 and 18 the corresponding velocity profiles. In particular, Figs. 17 and 19 suggest flow separation at 85% of the chord.

## CONCLUSIONS

An implicit procedure is developed for the solution of the incompressible Navier–Stokes equations in primitive variables. The implicit scheme of approximate factorization is used in the solution of the time dependent momentum equations for the velocity field while the pressure is computed from a Poisson type equation on a non-staggered grid. The analysis is presented in general curvilinear coordinates for a two-dimensional case since the extension to the three-dimensional case is straightforward. A consistent finite difference scheme, that is used and satisfies the compatibility condition of the pressure Poisson equation with Neumann boundary conditions, is developed in general curvilinear coordinates. A von Neumann stability analysis of the noniterative phase of the numerical scheme is conducted. Results are presented to demonstrate the excellent convergence and stability characteristics of the present method.

## ACKNOWLEDGMENT

The authors acknowledge the help of Mr. M. Metwally in the presentation of the results.

## REFERENCES

1. S. ABDALLAH, *J. Comput. Phys.* **70**, 182 (1987).
2. S. ABDALLAH, *J. Comput. Phys.* **70**, 193 (1987).
3. J. L. STEGER, *AIAA J.* **16**, 679 (1978).
4. S. J. SHAMROTH AND H. J. GIBLING, *AIAA J.* **18**, 1409 (1980).
5. J. H. PULLIAM AND J. L. STEGER, *AIAA J.* **18**, 159 (1980).
6. S. J. SHAMROTH, H. MCDONALD, AND W. R. BRILEY, *J. Eng. Gas Turbines Power* **106**, 383 (1984).
7. D. V. ROSCOE, S. J. SHAMROTH, AND H. MCDONALD, in *Computational Methods in Turbomachinery I MECH ENG CONFERENCE*, Publication 1984–3 (University of Birmingham, London, 1984), p. 67.
8. W. N. DAWES, in *Computational Methods in Turbomachinery I MECH ENG CONFERENCE* Publication 1984–3 (University of Birmingham, London, 1984), p. 157.
9. W. N. DAWES, "A Numerical Method for the Analysis of Three Dimensional Viscous Compressible Flow In a Turbine Cascade: Application to Secondary Flow Development in a Cascade With and Without Dihedral." *ASME Paper* 86-*GT*-145, 1986.

10. R. BEAM AND R. F. WARMING, *J. Comput. Phys.* **22**, 87 (1977).
11. R. F. WARMING AND R. M. BEAM, *SIAM-AMS Proceedings, Vol.* 11, 1978, p. 85.
12. W. R. BRILEY AND H. MCDONALD, *J. Comput. Phys.* **34**, 54 (1980).
13. R. W. MACCORMACK, *AIAA J.* **20**, 1275 (1982).
14. A. LERAT, *C. R. Acad. Sci. Paris A* **288**, 1033 (1979).
15. A. LERAT, "Sur le calcul des solutions faibles des systems hyperboliques des lois de conservation a l'aids de schemas aux differences," *ONERA Pub.* 1981–1, 1981.
16. W. KORDULLA AND R. W. MACCORMACK, *Lecture Notes in Phys., Vol. 170* (Springer-Verlag, New York/Berlin, 1982, p. 286.
17. A. LERAT, J. SIDES, AND V. DARU, *Lecture Notes in Phys., Vol. 170* (Springer-Verlag, New York/Berlin, 1982), p. 343.
18. W. R. BRILEY, H. MCDNALD, AND S. J. SHAMROUTH, *AIAA J.* **21**, 1467 (1982).
19. O. R. BURGGRAF, *J. Fluid Mech.* **24**, 113 (1966).
20. J. D. BOZMAN AND C. DALTON, *J. Comput. Phys.* **12**, 348 (1973).
21. S. G. RUBIN AND J. E. HARRIS, "Numerical Studies of Incompressible Viscous Flow in A Driven Cavity," *NASA SP*-378, 1975.
22. A. J. CHORIN, *J. Comput. Phys.* **2**, 12 (1976).
23. J. L. STEGER AND P. KUTLER, *AIAA J.* **15**, 581 (1977).
24. D. CHOI AND C. L. MERKLE, "Application of Time-Iterative Schemes to Incompressible Flow," *AIAA Paper* 84–1638, 1984.
25. A. RIZZI AND L. ERIKSSON, *J. Fluid Mech.* **153**, 275 (1985).
26. P. J. ROACHE, *Computational Fluid Dynamics* (Hermosa, Albuquerque, NM, 1982), rev. ed.
27. F. H. HARLOW AND J. E. WELSH, *Phys. Fluids* **8**, 2182 (1965).
28. J. E. WELCH, F. H. HARLOW, J. P. SHANNON, AND B. J. DALY, "The MAC Method" *LASL Report No. LA*-3425, Los Alamos Scientific Laboratory, Los Alamos, N. M. (1966).
29. W. R. BRILEY, "A Numerical Study of Laminar Separation Bubbles Using the Navier-Stokes Equation," *Report J*110614–1, United Aircraft Research Laboratories, East Hartford, CT (1970).
30. A. J. CHORIN, *Math. Comput.* **22**, 745 (1968).
31. R. S. BERNARD AND J. F. THOMPSON, "Approximate Factorization with an Elliptic Pressure Solver for the Incompressible Flow," *AIAA Paper* 82–0978 (1982).
32. R. SCHREIBER AND H. B. KELLER, *J. Comput. Phys.* **49**, 310 (1983).
33. H. VIVIAND, Conservative form of gas dynamics equations, *Rech. Aerosp.* **1**, 65 (1974).
34. M. VINOKUR, *J. Comput. Phys.* **14**, 105 (1974).
35. J. F. THOMPSON, Z. U. WARSI, AND C. W. MASTIN, "Numerical Grid Generation," *Lecture Notes On Numerical Grid Generation*, The Pennsylvania State University, May 1984.
36. G. OSWALD, "Analysis and Numerical Solutions of Unsteady Two-Dimensional Navier–Stokes Equations in Primitive and Derived Variables," M.S. thesis, University of Cincinnati, 1981 (unpublished).
37. J. F. THOMPSON, Z. U. A. WARSI, AND C. W. MASTIN, *Numerical Grid Generation Foundation and Applications* (Elsevier Science, New York, 1985).